Review

NMR Studies of RNA Dynamics and Structural Plasticity Using NMR Residual Dipolar Couplings

Melissa Getz,[1] Xiaoyan Sun,[1] Anette Casiano-Negroni,[1] Qi Zhang,[1] Hashim M. Al-Hashimi[1,2]
[1] *Department of Chemistry, The University of Michigan, Ann Arbor, MI 48109*
[2] *Biophysics Research Division, The University of Michigan, Ann Arbor, MI 48109*

Received 23 April 2007; revised 16 May 2007; accepted 16 May 2007
Published online in Wiley InterScience (www.interscience.wiley.com). DOI 10.1002/bip.20765

ABSTRACT:

An increasing number of RNAs are being discovered that perform their functions by undergoing large changes in conformation in response to a variety of cellular signals, including recognition of proteins and small molecular targets, changes in temperature, and RNA synthesis itself. The measurement of NMR residual dipolar couplings (RDCs) in partially aligned systems is providing new insights into the structural plasticity of RNA through combined characterization of large-amplitude collective helix motions and local flexibility in noncanonical regions over a wide window of biologically relevant timescales (<milliseconds). Here, we review RDC methodology for studying RNA structural dynamics and survey what has been learnt thus far from application of these methods. Future methodological challenges are also identified. © *2007 Wiley Periodicals, Inc. Biopolymers 86: 384–402, 2007.*

Keywords: RNA folding; RDC; adaptive recognition; collective motions; metal binding

Correspondence to: Hashim M. Al-Hashimi; e-mail: hashimi@umich.edu
Contract grant sponsor: NIH
Contract grant number: RO1 AI066975-01
Contract grant sponsor: NSF-CAREER
Contract grant number: MCB 0644278

This article was originally published online as an accepted preprint. The "Published Online" date corresponds to the preprint version. You can request a copy of the preprint by emailing the Biopolymers editorial office at biopolymers@wiley.com

RNA DYNAMICS AND CONFORMATIONAL ADAPTATION

Our view of ribonucleic acids (RNA), both in terms of their roles in gene expression and regulation and biophysical characteristics, has undergone a major transformation in the last decade. A universe of noncoding RNAs that carry out diverse functions is being uncovered, challenging the long-standing belief that proteins are the main gene product in living organisms.[1–5] Concurrently, X-ray, NMR, and other biophysical techniques are revealing three-dimensional RNA structures, such as those of the recently discovered riboswitches[6] that rival proteins in their structural complexity and functional sophistication.[7,8] An emerging theme is that RNA manages to achieve greater functional prowess by having a remarkable ability to undergo large conformational changes in response to specific cellular signals.[9–12]

Cellular signals that can induce changes in RNA conformation include recognition of proteins and small metabolite molecules, metal binding, changes in temperature, and RNA synthesis itself.[9–13] RNA conformational transitions generally serve specific biological functions. For example, stepwise changes in RNA conformation that are induced by successive protein recognition events make it possible to assemble complex ribonucleoproteins (RNPs) in an ordered hierarchical manner. Following folding and assembly, an RNA element will typically undergo yet another set of conformational changes to carry out its functions. For example, ribozymes undergo conformational changes during their catalytic cycles

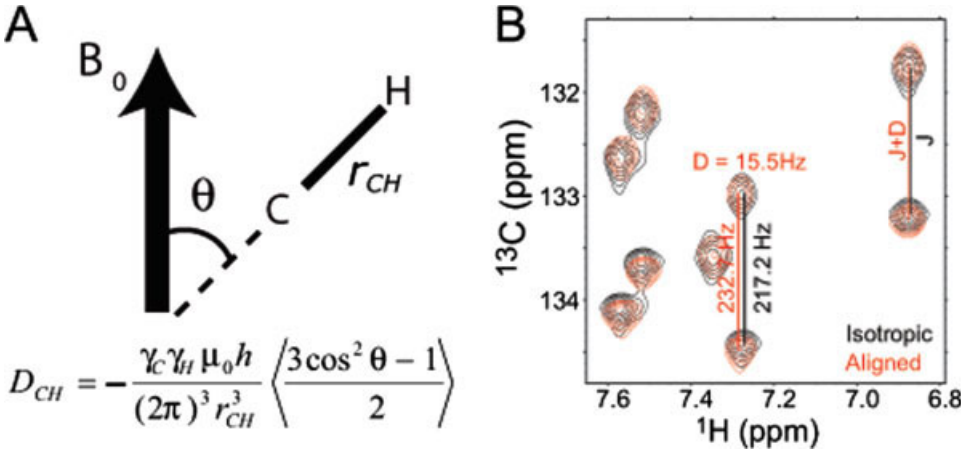

FIGURE 1 (A) Residual dipolar couplings between spins *i* and *j* provide long-range constraints on the average orientation (θ) of the internuclear bond vector relative to the applied magnetic field (B_0). (B) Measurement of residual dipolar couplings as new contributions to splittings of resonances observed upon partial molecular alignment.

in order to satisfy the diverse structural requirements of substrate binding, catalysis, and product release. RNA conformational changes also provide a basis for sensing signals and transmitting regulatory responses. The aforementioned riboswitches regulate gene expression by changing conformation in response to binding of small metabolite molecules or even changes in temperature.[6,13,14] The process of RNA synthesis itself can yield short-lived kinetically trapped intermediates that serve diverse functions.

The conventional view that one sequence codes for one structure that carries out a specific function must be replaced with a new paradigm in which an RNA sequence codes for many conformers, any of which can be stabilized adaptively depending on the cellular/physiochemical context. This in turn calls for the development and application of biophysical techniques that go beyond determination of static RNA structures under one set of conditions and that allow characterization of structure and dynamics at atomic resolution under a variety of conditions of interest.

Here, we review developments in NMR methods that rely on the measurement of residual dipolar couplings (RDCs) that provide unique insight into RNA structural dynamics. We focus on applications in which RDCs were used in the characterization of RNA structural plasticity, including collective motions of helical domains and local flexibility in noncanonical regions. Studies so far reveal a range of internal motions in RNA that can play diverse roles in their dynamical functions.

RESIDUAL DIPOLAR COUPLINGS

The theory underlying dipolar and other anisotropic interactions has been described in several places, including in the early liquid crystal applications[15–25] as well as in more recent reviews that deal specifically with biomolecular applications.[26–32] Here, we provide a brief description of the basic underpinnings of the methodology, with an emphasis on its application to nucleic acids.

The Dipolar Interaction

Nuclear dipole–dipole interactions arise from having the local field at a given nucleus that can be modulated by the nuclear magnetic flux emanating from a neighboring nucleus. An expression (in Hz) for this local field contribution between two spin ½ nuclei (*i* and *j*) is given by the dipolar interaction (D_{ij}),

$$D_{ij} = -\left(\frac{\mu_0}{4\pi}\right)\frac{\gamma_i\gamma_j h}{2\pi^2 r_{ij,\mathrm{eff}}^3}\left\langle\frac{3\cos^2\theta - 1}{2}\right\rangle, \qquad (1)$$

where μ_0 is the magnetic permittivity of vacuum, h is Planck's constant, r_{ij} is the internuclear distance between the spins, and γ is the gyromagnetic ratio. The angular term in Eq. (1) is the familiar second rank Legendre function, $P_2(\cos\theta_{ij})$, and is a function of the angle θ between the internuclear vector and the applied magnetic field (Figure 1A). The dipolar interaction is rendered time-dependent due to variations in the angle θ caused by overall molecular tumbling and internal motions. The angular bracket around the angular term denotes a time average over all angles sampled by the internuclear vector while an effective bond length, $r_{ij,\mathrm{eff}}$, subsumes the effects of distance averaging.

Motional averaging will generally reduce the value of the angular term and thus the magnitude of observed dipolar

couplings (which can be on the order of kiloHertz for non-reorienting directly bonded spins). When overall tumbling is random, the angular term averages to zero, explaining why dipolar couplings are normally not observed under solution conditions. However, if a degree of alignment can be imparted on the solute of interest, the angular term will no longer average to zero. The greater the degree of alignment the greater the value of the angular term and magnitude of observed dipolar couplings. As is the case for through-bond scalar couplings (J), through-space dipolar couplings (D) effectively increase or decrease the average magnetic field at a given nucleus, resulting in splitting of resonances. Dipolar couplings are therefore often measured as new contributions to scalar couplings (J) that are observed under conditions of molecular alignment ($J+D$) (Figure 1B).

The promise of RDCs in studies of RNA emanates primarily from the angular dependence in Eq. (1). First, RDCs can provide information regarding the orientational distribution of bond vectors relative to a common magnetic field direction, and hence relative to one another. This long-range angular information is highly complementary to traditional short-range interproton distance and dihedral constraints obtained from NOEs and scalar couplings, respectively. This proves to be particularly valuable in defining the conformation of extended nucleic acids that have a paucity of protons and NOEs. The orientational information can also be obtained with great abundance, because unlike NOEs, RDCs can be measured between a variety of spins (C—H, C—C, C—N, N—H, P—H, etc). Second, it is particularly straightforward to translate RDCs into information regarding both the average orientation and dynamics of molecular fragments that have known conformation. This proves to be an excellent match with the modular nature of RNA architecture in which the relative orientation of known helical domains is often of great interest but very difficult to characterize reliably using conventional NMR methods. Finally, RDCs are sensitive to motions occurring over a wide window of biologically important timescales (<milliseconds) and can provide information about the amplitude, asymmetry, and direction of motions.

Molecular Ordering and the Order Tensor

The interpretation of RDCs in terms of the internal structure and dynamics of a molecule typically requires specification of an order or alignment tensor that describes overall alignment of the molecule relative to the applied magnetic field.[23] The order tensor consists of five independent parameters. Two principal order parameters[33] define the degree ($\vartheta = \sqrt{\frac{2}{3}(S_{xx}^2 + S_{yy}^2 + S_{zz}^2)}$, $|S_{zz}| \geq |S_{yy}| \geq |S_{xx}|$) and asymmetry $\left(\eta = \frac{|S_{yy} - S_{xx}|}{S_{zz}}\right)$ of molecular alignment; two angular parameters define the average orientation of the magnetic field relative to the chiral molecular frame (the principal direction, S_{zz}), and a third angular parameter defines the orientation of an orthogonal principal axis (S_{yy}) that specifies the asymmetry of alignment.

The time-averaged angular term in Eq. (1) can be expressed in terms of the time-independent orientation of an internuclear vector relative to an arbitrary frame (α) and the five-order tensor elements (S_{kl}),[23,34]

$$\left\langle \frac{3\cos^2\theta - 1}{2} \right\rangle = \sum_{kl=xyz} S_{kl}\cos(\alpha_k)\cos(\alpha_l), \qquad (2)$$

where α_n is the angle between the internuclear vector and the nth axis of the arbitrary frame. Frequently, the order tensor is expressed in terms of a magnitude, D_a and rhombicity R,

$$D_a^{ij} = -\left(\frac{\mu_0}{4\pi}\right)\frac{\gamma_i\gamma_j h}{2\pi^2 r_{ij}^3}\left(\frac{1}{2}S_{zz}\right), \qquad R = \frac{2}{3}\eta \qquad (3)$$

PARTIAL ALIGNMENT OF NUCLEIC ACIDS

The measurement of RDCs in solution NMR is contingent upon inducing an appropriate degree of alignment.[35] Alignment levels $\leq 10^{-5}$ (i.e. ~1 in 10,000 molecules are on average completely aligned) leading to RDCs that are too small (compared to NMR line widths) to allow measurements at a useful level of precision. At much higher degrees of alignment ($\geq 10^{-2}$), RDCs can become unfavorably large with extensive dipolar couplings compromising the spectral resolution needed to analyze large biomolecules. In general, an optimum compromise is achieved for degrees of alignment on the order of 10^{-3}. Under these conditions, many RDCs can be measured with an optimal magnitude/precision ratio and with minimal sacrifice in spectral resolution. Alignment on the order of 10^{-4} can allow measurements of a smaller subset of RDCs with suboptimal magnitude/precision ratios.

Ordering Media Induced Alignment

Alignments on the order of 10^{-3} can now routinely be obtained in solution NMR by dissolving biomolecules in inert ordered media (for reviews see Refs. 36, 37). These ordered media can transmit some of their order to solute molecules through mechanisms that are believed to involve a combination of steric obstruction and charge–charge interactions (Figure 2A). This was first demonstrated for liquid crystalline disc-shaped phospholipids called "bicelles,"[38]

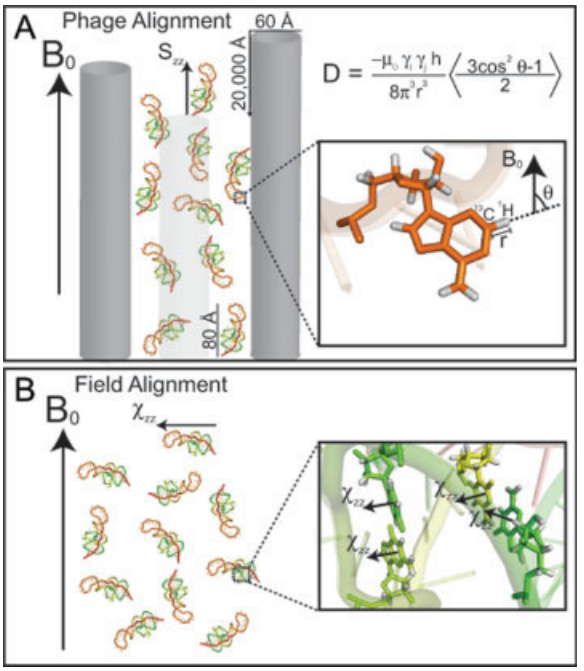

FIGURE 2 Partial alignment of nucleic acids using (A) ordering media such as Pf1 phage, which transmit their order through a combination of steric and electrostatic mechanisms and (B) spontaneous alignment due to constructive addition of anisotropic magnetic susceptibility tensors (χ) in the nucleobases of nucleic acids.

which were originally used as a mimic of membrane bilayers in studies of membrane-associated biomolecules.[39,40] While the original neutral bicelle medium has been employed in studies of nucleic acids, other media that have since been introduced have become more popular. In Table I, we provide a summary of ordering media used to date for aligning nucleic acids.

In general, media with high tolerance to ionic strength are desired for nucleic acid applications. Positively charged ordering media may not be a good choice as this may lead to unfavorable interactions. The most widely used medium is the filamentous bacteriophage (Pf1; Figure 2A).[42–44] Pf1 phage is composed of a 7.4-kb circular, single-strand DNA genome with one coat of protein per nucleotide. The molecules have a rod-like shape and are estimated to be ~20,000 Å long and ~60 Å in diameter.[44] The Pf1 medium is very robust having favorable properties in large part due to its lower nematic threshold concentration.[51,52] It is negatively charged, reducing the possibility for adverse interactions with nucleic acids. It induces alignment through electrostatic and steric mechanisms.[52,53] Owing to the uniform distribution of charge in polyanionic nucleic acids, the steric and electrostatic forces are believed to have a similar functional form.[52,53] Consequently, nucleic acids generally align in ordering media with the principal direction of order (S_{zz}) oriented along the long axis of the molecule. In general, one expects positive alignment ($S_{zz} > 0$) with the S_{zz} direction being, on average, oriented parallel to the magnetic field. Experimentally, RDCs are computed from the difference in splittings measured in the absence and presence of ~20–25 mg/ml Pf-1 phage (Figure 1B). The phage concentration can be estimated either by dividing the observed deuterium residual quadrupolar splitting by a factor of 0.886 or from the UV absorbance at 270 nm using the extinction coefficient of 2.25 cm ml/mg.[44]

Other media used to date in studies of nucleic acids include the neutral nonionic phase formed by use of alkyl–polyethylene glycol and *n*-hexanol.[49] This phase is robust to wide variations in pH, temperature, and ionic strength and is

Table I Alignment Media Used in Studies of Nucleic Acids

Ordering Medium	Temperature Range (°C)	Notes
DMPC:DHPC ("Bicelles")[38,41]	27–45	Perpendicular alignment disc-like shape. Neutral, sensitive to ionic conditions. The charge can be modified to be positive or negative with addition of CTAB or SDS, respectively. More stable ether-based bicelles can also be prepared
Rod-shaped viruses (Pf1 phage and TMV)[42–44]	5–60	Parallel alignment rod-like shape. Negatively charged, stable in pH higher than 5, and aggregates at high salt concentration. Sample is recoverable. Most widely used
Purple membrane[45,46]	−269 to 69	Parallel alignment disc-like shape. Stable in pH range 2.5–10, and salt concentrations up to 5*M*. Sample is recoverable
Polyacrylamide gels[47,48]	5–45	Mechanical gel. Very stable and inert. The charge can be modified to be positive or negative with addition of DADMAC or acrylate, respectively. Sample is recoverable
n-Alkyl-poly(ethylene glycol)/*n*-alkyl alcohol or glucopone/*n*-hexanol (PEG)[49,50]	0–40	Perpendicular alignment lamellar shape. Insensitive to pH, and moderately sensitive to salt concentrations

believed to induce alignment through a steric mechanism (Table I). Alternatively, stretched or compressed polyacrylamide gels[47,48,54] have also been used to align nucleic acids. Unlike the aforementioned liquid crystalline media, where the degree of solute order can be varied by changing the ordering medium concentration, the degree of solute alignment in polyacrylamide gels can be tuned by either modifying the gel density or by adjusting the amount of anisotropic strain or compression. A disadvantage is that any strain inhomogeneities will lead to line broadening, as different regions of the NMR sample experience different degrees of order and hence magnitudes of RDCs. An advantage is robustness over extreme conditions.

For proteins, it has been shown that different ordering media can lead to distinct solute alignments and allow measurements of independent sets of RDCs.[55,56] This can significantly expand the amount of structural and dynamical information that can be retrieved.[55–58] In contrast, to date there has been no example demonstrating modulation of nucleic acid alignment through use of different ordering media, even though attempts have been reported.[59] It is not surprising that nucleic acids exhibit greater tolerance for changes in alignment, given that the negative charge distribution closely follows that of excluded volume. Because advantages can be gained from measuring independent RDC sets, the development of approaches for modulating nucleic acid alignment is an important area of future development. As we discuss in what follows, magnetic field alignment offers one such possibility. Another may come from systematically elongating the RNA.[60]

Magnetic Field-Induced Alignment

An alternative approach for aligning nucleic acids involves spontaneous alignment due to interactions with the magnetic field itself. Initial efforts for measuring anisotropic interactions in biomolecules relied on spontaneous field alignment of molecules having large magnetic susceptibility anisotropies ($\Delta\chi$). Nucleic acids and paramagnetic proteins were primary biomolecular targets for these early investigations.[61–65] In nucleic acids, the diamagnetic susceptibility is dominated by the aromatic groups of base residues, wherein circulation of π-orbital electrons in response to the magnetic field results in an induced dipole moment that can reinteract with the magnetic field, and consequently cause an anisotropic preference in molecular orientation (Figure 2B). The degree of alignment and hence magnitude of RDCs depends on the diamagnetic susceptibly anisotropy ($\Delta\chi$) and, importantly, on the square of the magnetic field strength (B^2_0). Although the magnetic susceptibilities of individual bases are not sufficiently large to induce a useful degree of alignment ($\sim$2–7 $\times$ 10^{-6} at 800 MHz), their constructive addition, especially in A-form helices, in which bases are nearly coaxially stacked, can enhance the total anisotropy and resulting degrees of order (typically 10^{-4} at field strength of 800 MHz) (Figure 2B). The net principal χ-tensor direction (χ_{zz}) will be oriented nearly along the long axis of the molecule although this direction can deviate from the S_{zz} direction expected, based on the excluded volume in ordering media. Furthermore, unlike ordering media, one generally expects the diamagnetic alignment of extended nucleic acids to be negative ($\chi_{zz} < 0$) with the χ_{zz} direction being, on average, oriented perpendicular to the magnetic field noting that it is possible to have conformations that give rise to positive alignment ($\chi_{zz} > 0$).

For magnetic field-induced alignment, the degree of alignment can be expressed in terms of the magnetic field strength (B_0), the χ-tensor (in units of m^3/molecule), and temperature (T),[15,16,24,25]

$$S_{zz} = \Delta\chi\left[\frac{B_0^2}{15\mu_0 kT}\right] \quad \text{and} \quad S_{xx} - S_{yy} = \delta\chi\left[\frac{B_0^2}{10\mu_0 kT}\right],$$

where

$$\Delta\chi = \chi_{zz} - \left(\frac{\chi_{xx} + \chi_{yy}}{2}\right) \quad \text{and} \quad \delta\chi = \chi_{xx} - \chi_{yy}. \qquad (4)$$

The measurement of magnetic field-induced RDCs is somewhat different from that involving ordering media. Here, one measures splittings at different magnetic field strengths (preferably three or more). Back extrapolation of a linear plot of observed splittings versus B^2_0 is then used to determine isotropic scalar couplings (J), i.e. splittings at zero field (Figure 3). The RDCs at a given field strength (typically the highest field) are obtained by subtracting the computed scalar couplings (J) from the observed splittings ($J+D$; Figure 3). Apparent field RDCs can also be measured from the difference in splittings at two magnetic fields, but Eq. (4) must be adjusted accordingly.[66] It should also be noted that splittings have a contribution from dynamic frequency shifts (DFS), which arise from the imaginary component of the spectral density function for cross-correlation between dipolar and CSA relaxation mechanisms.[67,68] Fortunately, at magnetic fields above 400 MHz, the DFS contribution to the apparent splittings is nearly constant (within 0.1 Hz), resulting in a relatively small contribution to the measured RDCs (typically $<$0.2 Hz for C—H and N—H RDCs measured at fields $\geq$500 MHz).

The first observation of field-induced RDCs in nucleic acids dates back to 1987 in studies by Bothner-By and co-

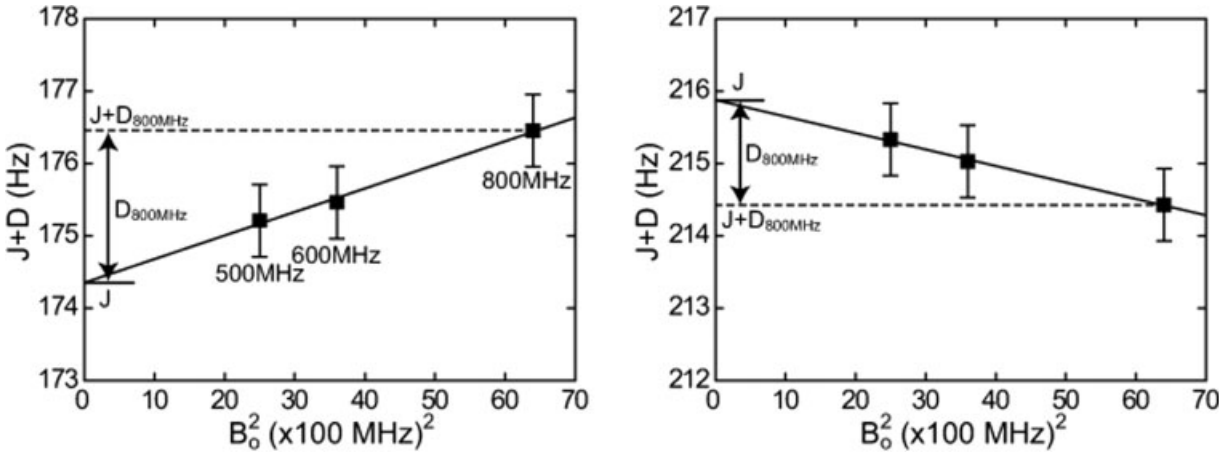

FIGURE 3 Two examples showing the measurement of magnetic field-induced RDCs from the quadratic dependence of splittings on B^2_0.

workers.[61] Magnetic field-induced RDCs were observed between H5 and H6 protons in two cytosine residues located at the center and terminal end of a DNA double helix. From these dipolar contributions, an angle of 15° between the cytosine base planes was inferred, suggesting loosening of the double helix at the ends of the strands.[61] Nearly a decade later, Bolton and coworkers demonstrated measurements of heteronuclear C—H field-induced RDCs in duplex and quadruplex DNAs.[62] Two years later, Bax, Tjandra, and coworkers[64] demonstrated the utility of measuring field RDCs in biomolecular structure refinement of a protein-DNA complex. Here, the magnetic anisotropy of the DNA was the primary source of the complex alignment. Together, these studies established the feasibility and utility of measuring RDCs in magnetically aligned nucleic acids.

Even with current magnetic field strengths, the achievable degree of magnetic field alignment (10^{-4}) for typical RNA constructs studied by NMR (20–40 nt) remains approximately an order of magnitude smaller than the optimum value (10^{-3}). However, even in these cases, magnetic alignment can offer a number of advantages, and interest in its application has been rejuvenated in recent years. For example, magnetic field-induced RDCs allow studies of structural dynamics in the absence of a potentially perturbing ordering medium. This can be important for highly flexible RNAs, which can have structures that are exquisitely susceptible to environmental conditions. Two studies thus far, one examining the structure of a DNA quadruplex[69] and the other the conformation of a flexible stem-loop TAR RNA,[70] using a combination of field and Pf1 phage-induced RDCs argue that the phage medium does not impact the structural integrity of nucleic acids.

Magnetic alignment can also offer an opportunity to modulate nucleic acid alignment relative to that induced by ordering media. While alignment in ordering media depends on global RNA shape, field alignment depends on the relative orientation of base groups, and these two properties are not always coincident.[16,25,64,69] For example, while the former ordering depends on the translational disposition of base-groups, the latter does not. That field alignment can result in distinct alignments relative to those induced by phage-ordering media was first demonstrated on a C2 symmetric DNA quadruplex.[69] Shown in Figure 4 is the experimentally determined orientation of alignment for the two cases. Clear differences in field and phage-induced alignment orientations are observed, with the principal direction of order being along the collective base plane direction in the case of field alignment (χ_{zz}) and along the long axis of the molecule in the case of phage alignment (S_{zz}). It has also been demonstrated that the magnetic field alignment of the stem-loop HIV-1 TAR RNA differs from that induced by the Pf1 phage.[70] Computational simulations suggest that field and phage will often yield different alignment orientations (Zhang and Al-Hashimi, unpublished results).

Finally, the χ-tensor governing field alignment has a simple dependence on molecular conformation. This can allow calculation of the total χ-tensor based on a known structure as well as derivation of simple expressions relating structure to alignment.[16,25,64,69] This can allow use of magnetic field-induced RDCs in determining nucleic acid stoichiometry,[71] in deriving the relative orientation of nucleic acid–protein complexes in cases where the nucleic acid structure is known,[64,72] aid structure determination,[66] and allow better analysis of conformational dynamics.[70] For such applications, having accurate knowledge of the base χ-tensor is of critical importance.[73]

Although the degree of field alignment remains smaller than optimal, there is reason to believe that optimal levels

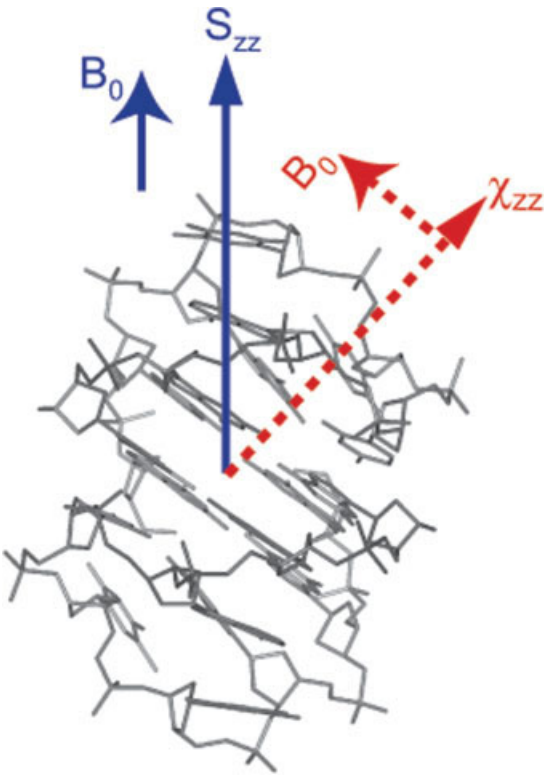

FIGURE 4 Comparison of phage (blue) and field-induced (red) alignment of a DNA quadruplex.[69]

will inevitably be reached as larger nucleic acids are investigated and magnetic field strength continue to rise. Shown in Figure 5 is the expected degree of alignment (ϑ) for RNAs of different size as a function of magnetic field strength. The upper bounds on the degree of alignment corresponds (filled symbols) to the case where all bases are coaxially stacked in an A-form helix, whereas the lower bounds (open symbols) correspond to the case where bases depart randomly from coaxial staking by an amount of 40°. As can be seen, the field-induced alignment could be achieved with optimum level (10^{-3}) at current field strength (900 MHz) for RNA on the order of 100 bp. NMR structures have been reported for RNAs as large as 100 nt.[74] Even larger RNAs, on the order of 150 bp, have been studied using NMR and segmental labeling strategies.[75] Thus we expect that with the development of higher magnetic field strengths, field-induced alignment will increasingly afford near optimum degrees of alignment for routine RNA RDC applications.

CHARACTERIZING RNA DYNAMICS USING RDCS

Several methods have been introduced for interpreting RDCs in terms of both structure and dynamics (reviewed in Refs. 31, 32, 37). Many of these methods, including model-free approaches for interpreting dynamics at the individual bond vector level pioneered by Griesinger and coworkers[58,76] and Tolman and coworkers[57,77] as well as more recent advances in the simulated annealing protocol[78,79] for refinement of structural ensembles[80,81] pioneered by Clore, have had limited applications to nucleic acids and thus will be not discussed here. The challenge in implementing the latter approaches is that they typically require the measurement of multiple RDC sets under independent alignment conditions, which as discussed earlier has proven difficult for nucleic acids. Overcoming this shortage in data is an important goal for the future.[81]

Relative Orientation and Dynamics of Helical Fragments

One of the first approaches for interpreting RDCs in terms of structure and dynamics proves to be of general utility in studies of RNA. In the so-called order tensor approach, and variants thereof,[33,34,82–86] order or alignment tensors are determined independently for locally rigid substructures in a target molecule. RNAs are by their very own nature modular structures that can be naturally decomposed into substructures consisting of locally stable A-form helices, the most abundant RNA secondary structure element. The determination of order tensors for individual helical fragments provides a natural approach for determining their relative orientation and dynamics. The orientation and dynamics of A-form helical domains is an important feature of RNA architecture that

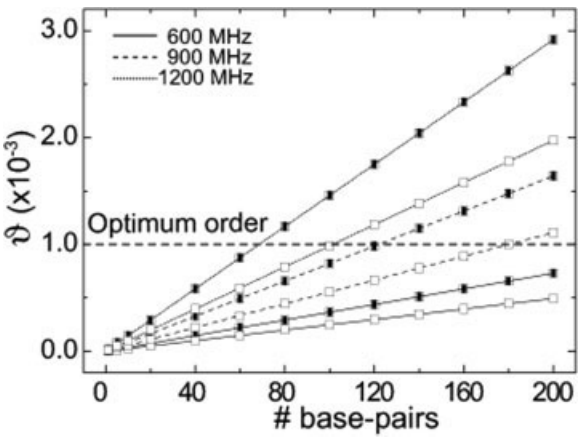

FIGURE 5 Computed degree of magnetic field-induced alignment of nucleic acids as a function of number of base-pairs and magnetic field strength. The base χ-tensors from Ref. 73 were used in these calculations. The filled symbols are upper bounds corresponding to the case of a perfectly linear A-form helix, and the open symbols correspond to structures with random distribution for nucleobases within a cone radius angle of 40°.

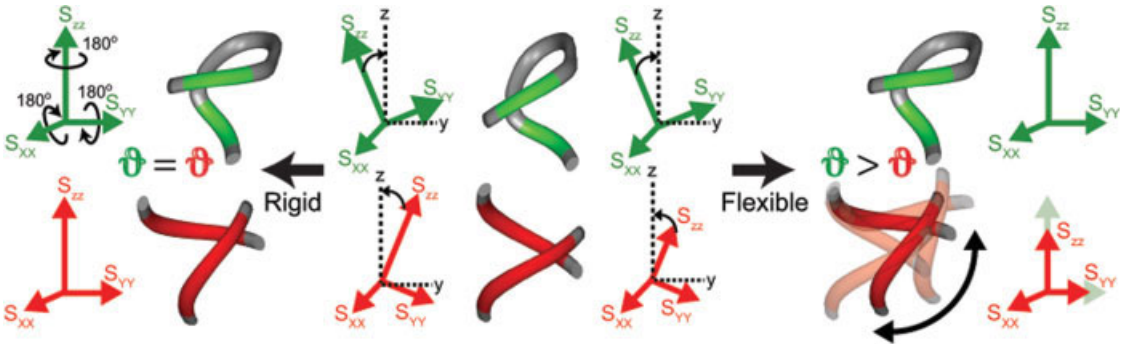

FIGURE 6 Order tensor analysis of RDCs in the determination of the relative orientation and dynamics of A-form helices in RNA. Order tensor frames (S_{xx}, S_{yy}, S_{zz}) are determined for individual helical fragments. Their average relative orientation is determined by superimposing their order tensor frames. Comparison of the degree of order determined for each helix allows characterization of interhelix motional amplitudes.

goes through mechanistically important changes during folding, recognition, and catalysis. It is also a feature of RNA architecture that is prone to artificial distortions from crystal packing forces. Although the approach by which order tensors are experimentally determined can differ, how this leads to determination of the relative orientation and dynamics of helical fragments is basically similar as summarized later.

The average orientation of helical domains can be obtained by superimposing their order tensor frames (Figure 6).[33,34,85] The analysis amounts to insisting that helical fragments share, on average, a common view of the magnetic field direction when assembled into a proper structure—similar to how countries in a properly assembled map report a common compass bearing. However, unlike compass bearings, one cannot distinguish between "positive" and "negative" directions along the principal axes of the order tensor (analogously between North/South and East/West). In other words, RDCs are degenerate to 180° rotations around the principal directions of the order tensor (S_{xx}, S_{yy}, and S_{zz}). This results in 4^{n-1} fold degeneracy in orienting n fragments, which can often be overcome either by measuring RDCs under at least two different alignments[55,56] and/or more typically in nucleic acids, by incorporating additional experimental and nonexperimental restraints.[59,83,86]

The two principal order tensor parameters (ϑ and η) obtained for each helix can be compared to obtain information about relative helix motions over submillisecond timescales (Figure 6).[33] While helices will report identical parameters when they are rigid relative to one another, interhelix motions can lead to differences. Specifically, the degree of order for a given helix (ϑ) will be attenuated relative to the value observed for a helix that more strongly dominates total alignment, with the degree of attenuation increasing with motional amplitudes. The ratio of helix order, defined as the internal generalized degree of order ($\vartheta_{int} = \vartheta_i/\vartheta_j$; $\vartheta_i < \vartheta_j$), then provides a measure of motional amplitudes, with $\vartheta_{int} = 1$ corresponding to perfect rigidity and $\vartheta_{int} = 0$ to maximum motions. Although often difficult to determine reliably, the asymmetry parameter (η) can in principle provide insight into the directionality of interhelix motions with spatially isotropic (directionless) motions having a smaller effect on the relative helix η values compared to anisotropic (directional) motions.[33,85]

Experimental Determination of Order Tensors for Helical Fragments

In nucleic acids, two strategies have been developed and applied for interpreting RDCs in terms of the structure and dynamics of RNA. The most widely used approach involves a variant of the simulated annealing approach in which individual helical domains are allowed to have independent order and/or alignment tensors. Here, RDCs and other experimental and nonexperimental restraints are combined to simultaneously determine the local structure of molecular fragments as well as their order tensors.[84,87] The latter approach can be generally applied to a variety of RNA fragments, provided that a sufficient number of experimental restraints (including RDCs) are measured and care has been taken to exclude RDCs that may have been attenuated by local motions.

Alternatively, the idealized A-form helix geometry can be used to model contiguous stretches of nonterminal Watson-Crick (WC) base-pairs.[83,85] The validity of this approach was recently supported by a statistical survey[88] of 421 WC base-pairs in 40 unbound and bound RNA X-ray structures (solved with <3Å resolution) and the 2.4 Å X-ray structure of the ribosome.[89] This study showed that the local conformation of two or more nonterminal contiguous WC base-pairs can, for the purpose of determining order tensors using

RDCs, accurately be modeled a priori using a standard idealized A-form helix geometry.[90,91] These WC base-pairs can be experimentally identified/verified using NOESY connectivity and trans-hydrogen bond J_{NN}-COSY type NMR experiments for directly detecting N—H · · · N hydrogen bonds.[92,93] The study also developed approaches for taking into account structural noise in the A-form geometry in the determination of order tensors and provided evidence that local motions in such helical fragments will not compromise the accuracy of derived order tensors.

By obviating the need to solve the local helix structure, the idealized A-form helix geometry makes possible a number of applications. First, one can determine the relative orientation and dynamics of helices for RNAs that may be too large for complete high-resolution structure determination. Second, the order tensor analysis of RDCs can be conducted with high efficiency, making possible systematic studies of how RNA's global conformational dynamics varies in response to changes in environmental conditions.[86,94–97]

The Decoupling Approximation

Most formalisms used to analyze RDCs in terms of structure and dynamics, including the aforementioned order tensor analysis, assume that internal motions do not lead to correlated changes in overall molecular alignment.[33,70,77,85] There are now many NMR[60,70] and computational[98,99] studies showing that this assumption will often be violated in extended modular RNAs. It is important to appreciate how violations in the decoupling approximation may impact analysis of RDCs.

For A-form helical domains in RNA, the "decoupling limit" is satisfied when one helix dominates alignment (e.g. because it is infinitely long) or when helices are held rigid relative to one another (Figure 7A). In practice, the decoupling limit is seldom realized in cases where helix motions are present. On the other extreme, the motional coupling limit is defined as the case in which helix motions result in identical changes in the overall alignment experienced by each helix. The latter results in identical apparent degrees of order for each helix (Figure 7B).[70] An example would be bending motions of two identical helices around a direction that is perfectly perpendicular to the two helix axes (Figure 7B). Therefore, the observation of $\vartheta_{int} = 1$ does not rule out the presence of interhelix motions. It is also true, however, that having equivalent helices does not imply that they will have identical ϑs and that therefore $\vartheta_{int} = 1$ (Figure 7B). For example, twisting motions around the long axis of a given helix can result in a reduction of its ϑ without affecting the ϑ value observed in another helix. Perhaps the most common regime will be one in which an RNA has intermediate or

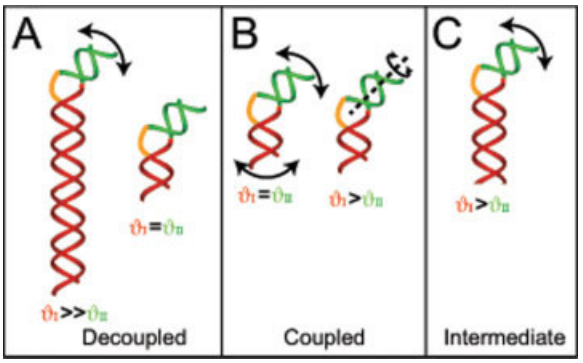

FIGURE 7 Various motional coupling regimes relevant to the structural and dynamical analysis of RDCs in nucleic acids.

residual motional couplings. Here, one helix partially dominates overall alignment. As a result, while the ϑ values observed for all helices will be attenuated by the helix motions, the attenuation will be smaller for the helix dominating alignment. Thus, the observed ϑ_{int} values will generally underestimate the real amplitude of interhelical motions.

Local Motions from Dynamically Attenuated RDCs

Insight into local motions of noncanonical residues can often be obtained from simple examination of the magnitude of measured RDCs.[32,37,100] In general, reorientation of bond vectors due to internal motions occurring at submillisecond timescales will lead to dynamical attenuation of the measured RDCs.[100] However, a near zero RDC value can also arise from static orientation of the internuclear vector relative to the order/alignment tensor, such as at the magic angle relative to the S_{zz} direction of an axially symmetric tensor. However, the observation of attenuated RDCs for many bond vectors in a given residue can, when combined with other structural information, be interpreted as evidence for local flexibility. Alternatively, local mobility can be inferred for regions that have RDCs that cannot be satisfied using a single structure during the structure determination process. In these cases, combination of RDCs with spin relaxation methods can be particularly useful for separating static and dynamic contributions to the RDC measurements.

MEASUREMENT OF RDCS IN NUCLEIC ACIDS

A large number of pulse sequences have been reported for the measurement of a wide variety of RDCs in nucleic acids. The pulse sequences are not reviewed here. Rather, we will survey the most commonly measured RDCs, particularly in applications aimed at determining the relative orientation and dynamics of A-form helices. Also not included in our discussion are the complementary measurements of residual

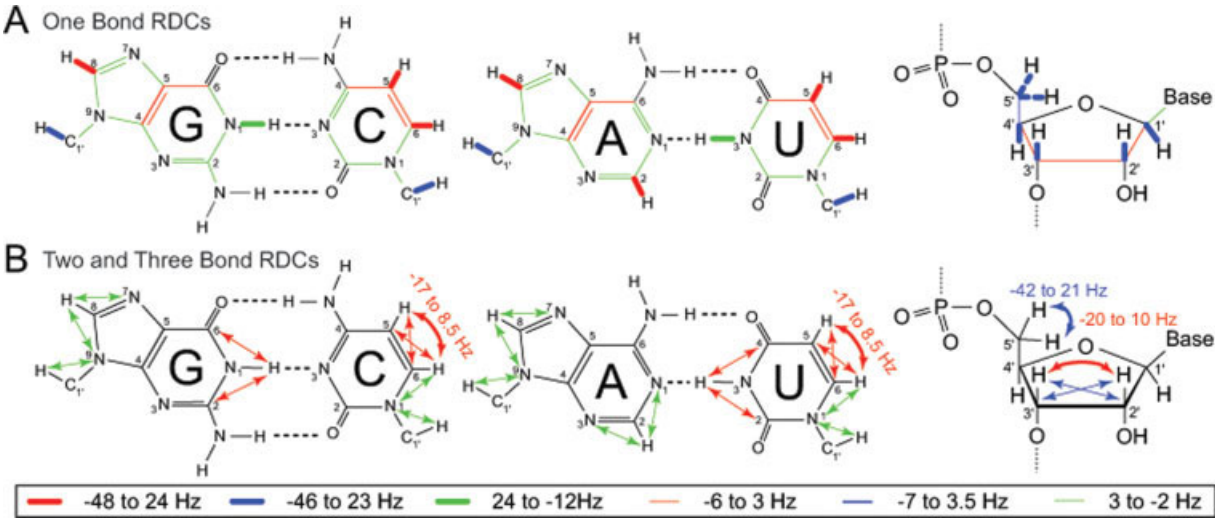

FIGURE 8 Typical RDCs measured in base and sugar moieties of RNA using the pulse sequences listed in **Table II**. (A) One bond C—H and N—H RDCs are the most commonly targeted interactions due to their favorable size, but smaller one bond C—C and C—N as well as (B) two and three bond RDCs can be measured.

chemical shift anisotropies, which can be measured abundantly and which offer new opportunities to study larger RNAs due to favorable TROSY effects.[101–104]

The most commonly measured RDCs in nucleic acids are shown in Figure 8 with example pulse sequences listed in Table II. The determination of order tensors for individual helices requires the measurement of at least five spatially independent (i.e. nonparallel) RDCs in each helical fragment. In practice, this requires the measurement of a larger number of RDCs, typically eight or more one bond C—H and N—H RDCs in both sugar and base moieties that yield a spatial distribution defined by a condition number (CN) < 5.[88] The choice of RDCs to be measured is guided by the desire to (i) maximize the magnitude: precision of measurement ratio, (ii) maximize spatial distribution of vectors, and (iii) minimize effects of structural noise and local motions.

The optimum and most commonly targeted RDCs are those between directly bonded C—H and N—H nuclei which yield the largest RDC magnitudes (Figure 8A). The effects of local motions and structural noise also appear to be favorably small for these interaction vectors.[88] Additional one, two, and three bond RDCs can also be measured (Figure 8B) using some of the pulse sequences listed in Table II. The latter RDCs are smaller and may prove difficult to measure in larger RNAs (>60 nt). It is noteworthy that as long as >8 RDCs are measured with CN < 5, the uncertainty in the order tensor due to A-form structural noise and RDC measurement uncertainty can be faithfully estimated.[88]

A minimum set of RDCs highlighted in Figure 9 consists of one bond C1′H1′, C2H2, C5H5, C6H6, C8H8, N1H1, and N3H3 vectors. These RDCs are attractive because they consist of nucleobase/sugar spins for which resonance assignments are typically the easiest to establish using NOESY and through-bound correlations (Figure 9).[116–118] There are also possibilities for integrating RDC measurements into the assignment process when the local helical fragment is known, thereby enhancing the efficiency and robustness of application even further.[85,86] Thus, while the order tensor analysis does not yield complete high-resolution structures, it bypasses the rate and size-limiting requirement for comprehensive assignments of resonances and NOEs, providing a basis for exploring the relative orientation and dynamics of helical domains under a variety of conditions of interest in large molecular systems.

RNA DYNAMICS FROM RDCS

There are now several studies that demonstrate the utility of RDCs in probing RNA structural dynamics. Here we survey a subset of studies that highlight different types of applications.

An early example was a study of the theophylline-binding RNA (TBR).[84] Here, structure refinement was undertaken in a series of steps starting with independent refinement of the local conformation of two domains against NOEs, scalar coupling constraints and RDCs, followed by refinement of the entire structure against all NMR constraints. The derived principal order parameters were very similar for the two domains, indicating that they are held rigid with respect to one another. However, five RDCs measured in the bulge nu-

Table II Pulse Sequences for the Measurement of C—H, N—H, C—N, C—C, H—H RDCs in Nucleic Acids

Pulse Sequence	Type of RDCs	Comments
HC[C](C) hd-TROSY-E.COSY[105]	$^1D_{C2H2}$, $^1D_{C5H5}$, $^1D_{C6H6}$, $^1D_{C8H8}$, $^1D_{C4C5}$, $^1D_{C5C6}$, $^2D_{C5H6}$, $^2D_{C6H5}$ and $^2D_{C4H5}$	Pseudo-3D experiments for homonuclear decoupling employing TROSY and E.COSY elements
CH_2-S^3E HSQC[106]	$^1D_{(C5'H5'+C5'H5'')}$ and $^2D_{(H5'H5'')}$ (in DNA only $^1D_{(C2'H2'+C2'H2'')}$ and $^2D_{(H2'H2'')}$)	2D experiments with spin-state selection for detection of up- or downfield carbon components of CH_2 spin states
3D S^3CT E.COSY[107]	$^1D_{C4'H4'}$, $^2D_{C5'H4'}$, $^1D_{(C5'H5'+C5'H5'')}$, $(^1D_{C5'H5'[']}-{}^2D_{H5'H5''})$, $^2D_{C4'H5'+C4'H5''}$, and $^3D_{H4'H5'[']}$	3D experiments for measuring RDCs in methine–methylene C—H pairs. One experiment yields 8 splittings
H1C1C2 E.COSY[108,109]	$^1D_{C1'H1'}$, $^1D_{C2'H2'}$, $^2D_{C1'H2'}$, $^2D_{C2'H1'}$, and $^3D_{H1'H2'}$	3D experiment utilizing E.COSY for measuring five splittings in one experiment
IPAP HN-HSQC, IPAP H(N)C-HSQC[110]	$^1D_{N1H1}$, $^1D_{N3H3}$, $^2D_{H1C2}$, $^2D_{H1C6}$, $^2D_{H3C2}$, and $^2D_{H3C4}$	2D experiments yielding 1-2 couplings per experiment
3D IPAP-HCcH-COSY, 3D relay-HCcH-COSY[109,111]	$^1D_{C2'H2'}$ and $^1D_{C3'H3'}$	Uses C1′H1′ to alleviate spectral overcrowding in the C2′H2′ and C3′H3′ region
MQ-HCN[112]	$^1D_{C1'H1'}$, $^1D_{C1'N1/N9}$, $^1D_{C1'C2'}$, $^2D_{H1'N1/9}$, $^2D_{H1'C2'}$, $^2D_{H1'N1/9}$, $^1D_{C6H6}$, $^1D_{C6N1}$, $^1D_{C6C5}$, $^1D_{C8H8}$, $^1D_{C8N9}$, $^2D_{H8N9}$, $^2D_{H6N1}$, and $^2D_{H6C5}$	Suite of six MQ based 3D experiments. One-two splittings per experiment
S^3E IS[T][113]	^1D and ^2D	2D experiments for measuring most of the one- and two-bond splittings
^{13}C-^{1}H TROSY[114]	$^1D_{C2H2}$, $^1D_{C5H5}$, $^1D_{C6H6}$, and $^1D_{C8H8}$	Sensitivity enhanced using TROSY and native ^{13}C magnetization
3D MQ/TROSY-HCN-QJ[115]	$^1D_{C1'N9}$, $^1D_{C8N9}$, $^1D_{C4N9}$, $^1D_{C1'N1}$, $^1D_{C6N1}$, and $^1D_{C2N1}$	3D quantitative J-modulated experiments for measuring one bond C—N splittings

cleotide C27 linking the two stems, which was believed to be flexible based on ^{13}C relaxation measurements, were found to be consistent with dynamical sampling of multiple rather than a single conformation (Figure 10).

Several studies have since qualitatively interpreted attenuation of RDCs and/or difficulties in inclusion in static structure refinement as evidence for local mobility. Representative examples are shown in Figure 10, with the locally mobile residues inferred from RDCs highlighted in purple. The locally mobile residues generally belong to loops, bulges, or base-pairs in short helical segments. They are often highly conserved and/or implicated in function. In some cases, local mobility at these sites seems to be important in allowing structural rearrangements to take place during molecular recognition.

For example, Puglisi and coworkers used a divide and conquer strategy involving combined use of RDCs and NOEs to characterize the structure and dynamics of a large (25 kDa) RNA comprising domain II of the hepatitis C virus (HCV) internal ribosome entry site (IRES) (Figure 10).[119] Domain II is part of the 5′ UTR of the virus and binds the 40S ribosomal subunit and controls translation. The domain IIa portion solved by NMR is shown in Figure 10. The study identified with the aid of RDCs local mobility at uridine bulges that may allow for minor conformational adjustments upon binding to the 40S.

Another example is a study of the stem-loop D (SLD) by James and coworkers. SLD is a hairpin loop located in the 5′ UTR of enterovirus and rhinovirus genomes (Figure 10). It is composed of three domains connected by a string of noncanonical pyrimidines and a two-residue AU bulge that was shown with the aid of RDCs to be highly flexible.[120] Flexibility at the AU bulge may also aid adaptive binding to cognate protein targets. More recently, Wijmenga and coworkers solved the structure of a highly conserved stem-loop at the 5′ end of the hepatitis B viral genome (HBV, Figure 10) using a combination of NOEs, RDCs, and ^{1}H chemical shift data.[121] A single U23 bulge residue that induces an average interhelical kink angle of $\sim 20^\circ$ was shown to be flexible, adopting two different conformations, one of which is likely important for protein recognition.

By increasing the number of measured RDCs, one can examine the structural dynamics of smaller molecular fragments using order tensor-like analyses.[82] Bax and coworkers used RDCs to characterize the conformational dynamics of H1′C1′C2′H2′ molecular fragments in the ribose sugars of a 24-mer RNA stem-loop derived from the helix-35 of *E. coli* 23S ribosomal RNA (Helix 35, Figure 10).[108] Determination of order tensors for such molecular fragments was made possible by a 3D NMR experiment that allows simultaneous

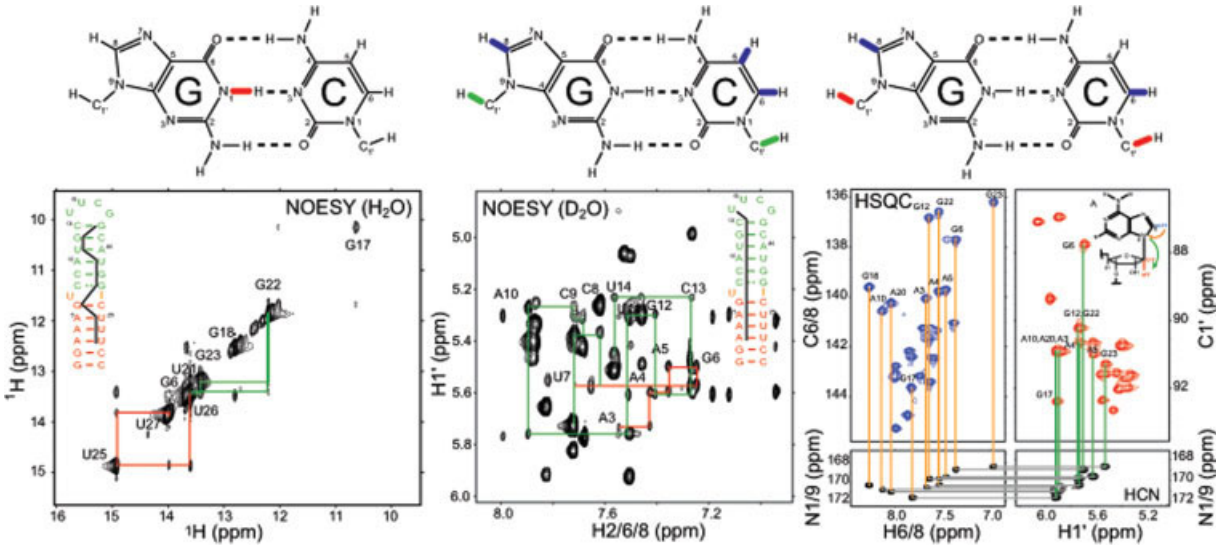

FIGURE 9 A minimum set of C—H and N—H RDCs in A-form helices involving nuclei that can be readily assigned using conventional NOESY and triple-resonance experiments.

measurements of the following RDCs: ${}^1D_{C1'H1'}$, ${}^1D_{C2'H2'}$, ${}^1D_{C1'H2'}$, ${}^1D_{C2'H1'}$, and ${}^1D_{H1'H2'}$ (Table II). Order tensors for such fragments could be determined for helical residues by assuming a standard C3′-endo ribose ring pucker conformation. Interestingly, while the degree of order was found to be similar for various residues in the helix, indicating molecular rigidity, a ∼15% reduction in degree of order was observed for the terminal nucleotide likely due to end fraying (Figure 10).

A study by Chen et al. nicely highlights how RDCs can be combined with spin relaxation and NOE data to obtain insight into local flexibility. This study reported on the structure and dynamics of the *Tetrahymena thermophila* stem-loop IV (SL-IV) RNA component of the telomerase enzyme (Figure 10).[122] Telomerase catalyzes the de novo addition of telomeric repeats that cap and protect the end of linear chromosomes and thereby enhance their genetic stability. SL-IV plays an essential role in telomerase folding, making major contributions to enzyme activity and to processivity of repeat addition. Dynamically attenuated RDCs were observed at two sites; two sets of AU residues in between a GA and U bulge, which were predicted to form base-pairs that could not be experimentally observed, and residues in the ACUAU apical loop. Exchange broadening was also observed at the A-U base-pairs supporting the presence of motions at these sites. In contrast, several residues in the apical loop exhibited elevated $T_{1\rho}$ times, particularly U135, indicating the presence of motions at ps-ns timescales. Interestingly, rigidifying the AU region through replacement with GC base-pairs resulted in two- to threefold reduction in enzyme activity and processivity. The authors proposed that the bending at the GA bulge together with flexibility in nearby regions may help reposition the apical loop during the enzyme catalytic cycle and may also play a role in RNP assembly.

Concurrently, Feigon and coworkers reported on the structure and dynamics of a variant construct of the *T. thermophila* SL-IVFragment (Figure 10).[123] This study provided additional insight into the dynamic nature of the global SL-IV structure. Order tensor analysis of RDCs measured in the two helical domains flanking the GA bulge, which employed an idealized A-form geometry, revealed a significant interhelical bend angle (∼50°) in excellent agreement with results from Chen and coworkers (interhelical bend angle of ∼43°). The order tensor analysis also revealed that the degree of order for the shorter lower stem is 15% smaller than that of the longer upper stem, suggesting the presence of interhelical motions. Analysis of the asymmetry parameter obtained for each helix suggested that the interhelical motions are highly directional.

Several RDC studies provide evidence for collective helix motions in RNA. Representative examples are also highlighted in Figure 10. Prior to the earlier telomerase studies, Leeper and Varani used RDCs to study the "CR4-CR5" domain (referred to as hTR J6), which is believed to be a functional counterpart of SL-IV in the vertebrate telomerase (Figure 10).[124] hTR J6 is composed of two helical domains joined by an internal loop containing two cytosine residues and an ACU sequence (Figure 10). Independent structure refinement of the two helical domains using RDCs provided evidence for a small difference in the degree of order for the two helical stems con-

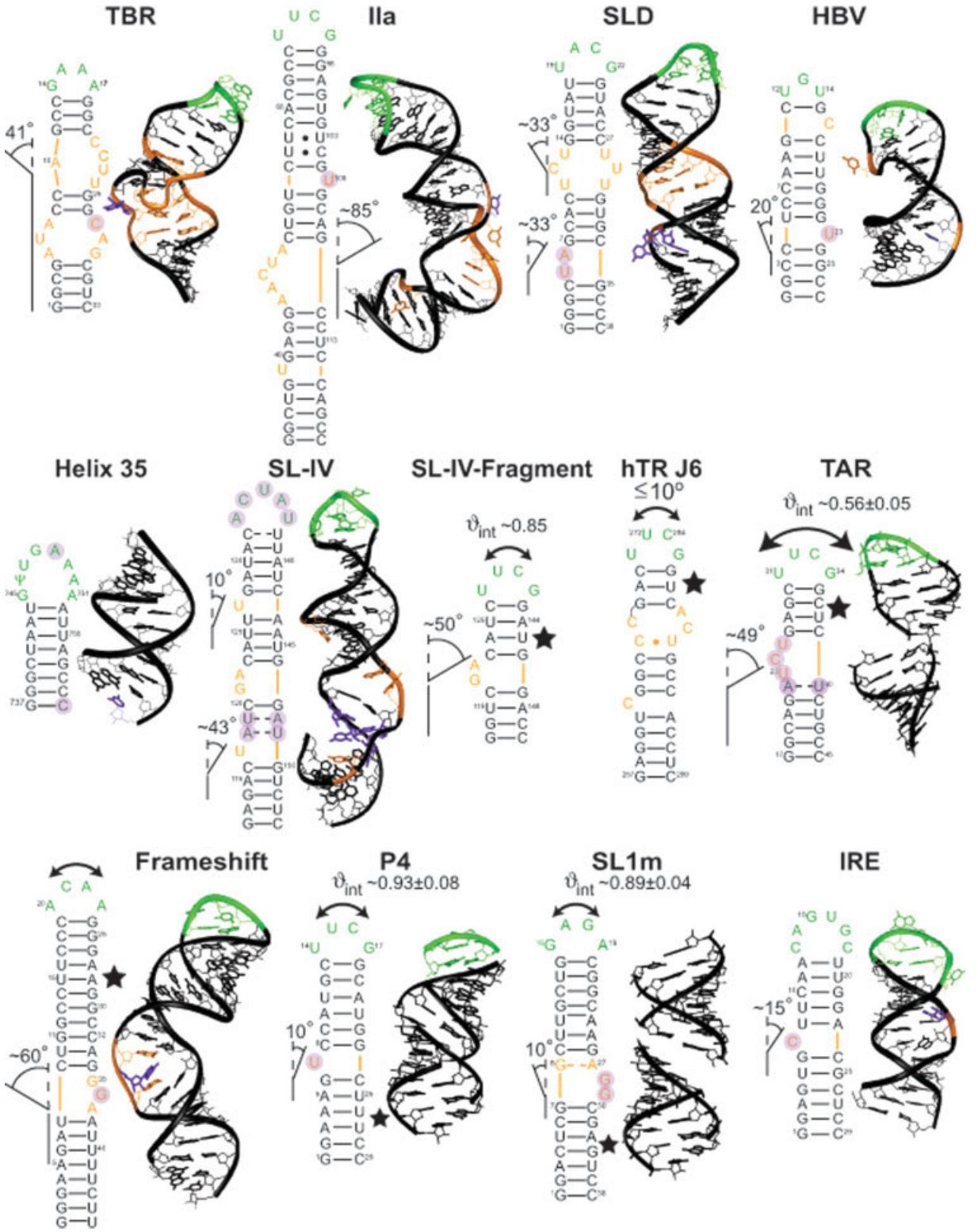

FIGURE 10

sistent with the presence of small amplitude ($\leq 10^{\circ}$) interhelix motions that likely correspond to a directional arc trajectory.

The first evidence for interhelix motions in RNA was provided in a study of the free state of an HIV-1 TAR RNA construct in which the wild-type apical loop was replaced with a

UUCG loop.[86] Previous NOE-based structures showed that while the two helices in TAR adopt a bent average conformation (~49°) in the free state, binding to peptides derived from its cognate transactivator protein target *Tat* leads to a conformation in which the two helical domains are far more coaxially aligned.[128,129] RDCs and the idealized A-form geometry were used to determine order tensors for each of the two TAR helices.[86] Superposition of the order tensor frames yielded an average interhelical angle, ranging between 44° and 54° in agreement with previous studies (Figure 10).[129–131] However, the degree of order observed for the lower helix I was significantly smaller than that observed for the upper helix II, indicating the presence of substantial interhelical motions. These results were interpreted as evidence that TAR may dynamically sample the linear conformations required for Tat recognition. More recent studies involving measurements of relaxation data in elongated TAR constructs provided additional support for interhelix motions and a mode of recognition involving tertiary structure capture.[60] The amplitude of helix motions obtained by spin relaxation (S_s = 0.85) were smaller than those obtained by RDCs (ϑ_{int} = 0.59), indicating that the helix motions occur at timescales slower than overall molecular tumbling of elongated TAR (τ_m = 18.9 ns). The RDCs measured in bulge residues C24 and U25 as well as the neighboring A22-U40 base-pair were also attenuated, consistent with a flexible interhelix linker. Independent support for local motions in these residues was also obtained from motional narrowing of resonances in elongated TAR constructs.[86]

Staple and Butcher examined the conformational dynamics of the frame-shift inducing element in HIV-1 (Figure 10).[125] This RNA contains a three-purine bulge (GGA) that induces an interhelical bend of 60°. The authors observed a different level of order for the two helices (~23% reduction for the lower stem), which indicates the presence of anisotropic directional interhelix motions involving rotations around an axis perpendicular to that of the plane of the two helices. As expected, the longer helix II dominated overall alignment. It is not known how these frame-shift inducing elements function, but in HIV-1, the lower stem significantly enhances frameshift efficiency. It has been noted in other RNAs that bending (and perhaps in the future, dynamics) is necessary for function of these frame-shifting elements. It is thought that the bend is needed for interaction with the ribosome during translation and the usually AU-rich bottom stem is denatured, leading to alternate base-pairing (frameshifting).

Collective helix motions have also been observed using RDCs between two helices in the RNase P P4 helix containing a single pyrimidine bulge nucleotide (Figure 10).[126] Idealized A-form helices were used to model nonterminal WC base-pairs in the two helices. The locally flexible and looped-out uridine bulge was found to induce a small average bend between the two helices (10°). A slightly smaller (~7%) degree of order was observed for the upper helix II (ϑ_{int} = 0.93) indicating the presence of interhelix motions. The interhelix motions were substantiated based on ^{15}N spin relaxation measurements in elongated P4 constructs.[126] Unlike TAR, the motional amplitudes obtained by spin relaxation (S_s = 0.95) were in very good agreement with values obtained by RDCs (ϑ_{int} = 0.93), ruling out the presence of interhelix motions at timescales slower than overall tumbling of elongated P4 (~19 ns). The dynamical hinge for interhelix motions was situated near a site of Mg^{2+} binding which may be important for RNase P catalysis. Given its central location in RNase P, local and collective helix motions in P4 may be important in allowing structural rearrangements to take place during folding and catalysis.

A similar order tensor analysis of RDCs combined with ^{15}N relaxation measurements in elongated constructs revealed the presence of collective motions between two helices in the HIV stem-loop 1 (SL1m) (Figure 10).[127] The two helices in SL1m are linked by a highly conserved four-residue internal loop, which induces a small average interhelical bend angle (10° ± 4°; Figure 10).[127] The upper helix II, which contains a series of melted base-pairs, exhibited a smaller degree of order relative to the lower helix (Figure 10).[127] Exchange broadening of resonances revealed a possi-

FIGURE 10 Representative studies probing local and collective motions in RNA using RDCs. Residues shown to be locally flexible using RDCs are highlighted in purple. Collective motions of helices are indicated using arrows. The helix that is observed to dominate alignment in the presence of collective motions is indicated with a star. Interhelical bend angles are also shown. The examples include the TBR,[84] domain II of HCV IRES (IIa),[119] SLD from the 5′ UTR of enterovirus and rhinoviruses genomes (SLD),[120] a stem-loop at the 5′ end of the HBV,[121], stem-loop derived from helix-35 of *E. coli* 23S ribosomal RNA (Helix 35),[108] *Tetrahymena thermophila* SL-IV RNA in two variant constructs (SL-IV)[122] and (SL-IV-Fragment),[123] the CR4-CR5 domain in the vertebrate telomerase (hTR J6),[124] HIV-1 TAR RNA,[86] the frame-shift inducing element in HIV-1 (Frameshift),[125] RNase P P4,[126] HIV SL1m,[127] and the iron-responsive element (IRE).[87]

ble secondary structural rearrangement occurring at μs-ms timescales involving the internal loop and base-pairs in the upper stem. It was proposed that the motions between the two helices together with secondary structural rearrangements might promote a functionally important structural rearrangement between kissing and duplex forms of the SL1 dimer.

The earlier examples suggest that the collective motions of RNA helical domains across flexible junctions may be a general property of RNA architecture. However, it should be stressed that the degree of helix motions present are likely underestimated due to presence of residual motional couplings (Figure 7). Thus, although in many cases no discernable differences in helix order are observed, this does not rule out the presence of interhelix motions. In cases where differences are observed, quantitative assessment of the motional amplitudes remains complicated by the possible presence of motional couplings.

INDUCED CHANGES IN CONFORMATIONAL DYNAMICS

Another exciting application of RDCs is in the characterization of how the structure and dynamics of RNA varies in response to changes in environmental conditions. These conformational changes are subtle and difficult to detect using conventional NMR or other spectroscopic methods. When combined with knowledge of RNA flexibility, these studies are beginning to shed light on how RNA structures adapt to perform their functions.

Metal-Induced Structural Transitions

The measurement of RDCs is allowing for the characterization of how metals affect the RNA conformation and dynamics when it is otherwise very difficult to establish based on conventional methods. This was first demonstrated for HIV-1 TAR RNA, in which an order tensor analysis of RDCs revealed that Mg^{2+} binding causes an arrest of interhelix motions and stabilization of a coaxial conformation (Figure 11)[94] similar to that observed in the X-ray structure determined in the presence of high concentrations of divalent ions.[132] This global structural change was accompanied by looping out of the otherwise stacked U23 and C24 bulge residues, which exhibited more attenuated RDCs in the presence of Mg^{2+}.[94,132] A more recent RDC study showed that Na^{+} ions induce a similar TAR structural–dynamical transition, although the mode of metal binding may differ from that of Mg^{2+}.[133]

The impact of Mg^{2+} on RNA conformation was also examined for the P4 helix and SL1m RNA mentioned earlier. In contrast to TAR, Mg^{2+} binding had an insignificant effect on the structure and dynamics of P4.[126] While Mg^{2+} also did not affect the average orientation of the two helices in SL1m, it led to a complete arrest of the interhelix motions.[127] This was accompanied by preservation and/or activation of local mobility at internal loop residues G272 and G273 which are implicated in binding the NC protein.

The aforementioned metal-induced changes in RNA conformation may be understood in terms of the interplay of electrostatic and base-stacking interactions. At low ionic strength conditions, interhelical bending serves in part to al-

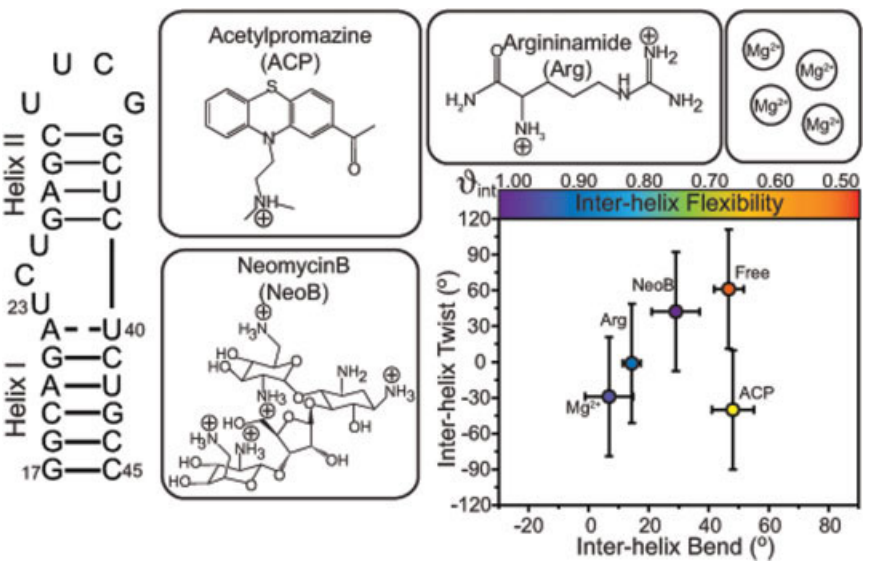

FIGURE 11 Probing changes in the conformational dynamics of HIV-1 TAR RNA upon binding to Mg^{2+} and small molecules.

leviate charge repulsion which would otherwise build up due to spatial confinement of backbone phosphates in the bulge/internal loop.[94,134–138] By screening charge repulsion, divalent and monovalent ions can help stabilize coaxial helical conformations. This in turn may require the looping out of bulge/internal loop residues that may be involved in stacking interactions, as observed in the case of TAR and SL1m. Thus, the energetic gains due to favorable coaxial helical stacking and metal binding have to offset the unfavorable loss of stacking interactions in bulge residues. In the case of P4, the uridine bulge was looped out, and the two helices nearly coaxially stacked in the absence of Mg^{2+} possibly explaining why Mg^{2+} had a substantially smaller effect on conformational dynamics.

Molecular Recognition

RDCs are also providing insight into changes in RNA conformation that are induced by molecular recognition. An early example was the use of RDCs to identify RNA conformational changes induced by binding to aminoglycosides.[139] Differences in the RDCs measured in two adenosines located in an asymmetric loop of the RNA in the free and antibiotic-bound forms nicely correlated with the known structural changes that were proposed to occur.

A series of studies employing an order tensor analysis of RDCs have examined how the relative orientation and dynamics of A-form helices in HIV-1 TAR change in response to binding of small molecules, most of which were designed to inhibit the TAR-Tat interaction. Previous NOE-based NMR studies had shown that TAR RNA undergoes conformational rearrangements upon binding to small molecules bearing a different number and spatial arrangement of cationic groups.[128,129,140–143] Figure 11 shows some of these TAR conformational transitions as visualized through application of an order tensor analysis of RDCs.[85,94–96] Interestingly, one finds that molecules that contribute a larger number of cationic groups tend to stabilize more linear and rigid TAR conformations (Figure 11), in analogy to the trend observed when adding metals (Mg^{2+}) as discussed earlier.

Chemical Modifications

RDCs have also been used to examine whether chemical modifications of interest affect the structure and/or dynamics of RNA. Butcher and coworkers used RDCs to examine the impact of phosphorothioate substitutions which are commonly used to elucidate functionally important metal-ion binding sites in RNA.[144] Specifically, they examined the impact of an S_p-phosphorothioate substitution at residue U80 in the U6 RNA stem-loop. This phosphorothioate substitution was previously used to demonstrate the presence of a metal-binding site at this location that is critical for spliceosome function. With the aid of RDCs, the authors solved and compared structures for U6 RNA with and without the phosphorothioate substitution. Because of difficulties in chemically preparing the modified RNA with ^{13}C and ^{15}N labeling, C—H RDCs were measured at natural abundance. Very similar structures were determined for the two RNAs, indicating that the single S_p-phosphorothioate substitution at residue U80 is structurally benign, validating use of phosphorothioate substitutions in identifying metal-binding sites.

Vermeulen et al. used RDCs to examine how posttranscriptional modifications affect the structure of $tRNA^{Val}$.[145] Although no major structural differences were observed, the RDCs measured at residues near sites of modifications exhibited significant differences between the modified and unmodified tRNA form, indicating that they have altered local conformations perhaps due to added steric restraints from the modifications.

Du et al. used RDCs to help examine how a single C10 to U10 mutation in the loop B region of SL-IV domain within the internal ribosomal entry site affects its structure and dynamics (Figure 10).[146] The loop B contains an unusually long six-nucleotide asymmetric bulge containing a stretch of three cytosine residues that is important for binding the PCBP2 protein and critical for *Poliovirus* translation. The C/U mutation targeted one of the cytosine residues in the bulge. Remarkably, although attenuated RDCs were observed for many bulge residues in the wild-type RNA, indicating the presence of extensive flexibility, these motional attenuations were nearly absent in the 10U mutant, indicating limited flexibility in the bulge. Structure determination of the two RNAs revealed that while the wild-type RNA adopts an overall "L"-shape conformation, the 10U mutant adopts an overall "U"-shape conformation. Although the biophysical basis for these dramatic changes in structure and dynamics are not fully understood, the authors speculate that the more rigid 10U RNA adopts a preformed scaffold for protein recognition, whereas recognition of the more flexible wild-type sequence requires conformational changes in the RNA.

SUMMARY

The measurement of RDCs is providing new insight into the dynamical properties of RNA structure. Inherent flexibility involving local motions of residues and collective movements of intact domains can now be characterized over a wide range of timescales. In several cases, these motions appear to serve the role of aiding RNA conformational transitions, including

adaptive formation of intermolecular interactions with cognate targets. The exquisite conformational sensitivity of RDCs is also providing new opportunities for carefully characterizing how RNA conformation changes in response to specific physiochemical changes, including recognition of molecular targets, metal binding, and chemical modifications. These studies suggest that even minor modifications in sequence or chemical context can lead to dramatic changes in the RNA conformational dynamics, further emphasizing the need to abandon the notions that one RNA sequence codes for a single structure.

There are a number of areas for future development. First, the ability to probe collective dynamics by RDCs remains complicated by the potential presence of unaccounted for motional couplings between internal motions and overall alignment. Techniques such as domain-elongation[60] can be used in the future to minimize these motional couplings and allow for more quantitative characterization of the amplitude, directions, and asymmetry of helix motions. Second, there is a need to develop approaches for modulating alignment of nucleic acids. Only then will it be possible to effectively apply model-free[58,77] and ensemble[81] approaches for the characterization of dynamics with enhanced structural resolution. Finally, the combination of RDCs with other techniques, including spin-relaxation methods and time-resolved NMR discussed in other review articles in this issue promises to lay a basis for unraveling the structural plasticity of RNA over the entire window of biologically relevant timescales.

We thank members of the Al-Hashimi lab for insightful comments and Dr. Alex Kurochkin for his expertise and for maintenance of the NMR instruments. We thank Maxamillian Bailor and Alexandar L. Hansen for Figures 6, 8, and 11. H. M. A. would like to acknowledge collaborations with the groups of Carol Fierke (The University of Michigan) and Ioan Andricioaei (The University of Michigan). The authors gratefully acknowledge the Michigan Economic Development Cooperation and the Michigan Technology Tri-Corridor for the support of the purchase of 600 MHz spectrometer.

REFERENCES

1. He, L.; Hannon, G. J. Nat Rev Genet 2004, 5, 522–531.
2. Ambros, V. Nature 2004, 431, 350–355.
3. Mello, C. C.; Conte, D., Jr. Nature 2004, 431, 338–342.
4. Hannon, G. J.; Rossi, J. J. Nature 2004, 431, 371–378.
5. Mattick, J. S. Nat Rev Genet 2004, 5, 316–323.
6. Mandal, M.; Breaker, R. R. Nat Rev Mol Cell Biol 2004, 5, 451–463.
7. Schwalbe, H.; Buck, J.; Furtig, B.; Noeske, J.; Wohnert, J. Angew Chem Int Ed Engl 2007, 46, 1212–1219.
8. Nudler, E. Cell 2006, 126, 19–22.
9. Williamson, J. R. Nat Struct Biol 2000, 7, 834–837.
10. Leulliot, N.; Varani, G. Biochemistry 2001, 40, 7947–7956.
11. Al-Hashimi, H. M. Chembiochem 2005, 6, 1506–1519.
12. Micura, R.; Hobartner, C. Chembiochem 2003, 4, 984–990.
13. Narberhaus, F. Arch Microbiol 2002, 178, 404–410.
14. Grundy, F. J.; Henkin, T. M. Curr Opin Microbiol 2004, 7, 126–131.
15. Bastiaan, E. W.; Maclean, C.; Van Zilj, P. C. M.; Bothner-By, A. A. Ann Rep NMR Spectrosc 1987, 19, 35–77.
16. Bastiaan, E. W.; MacLean, C. NMR Basic Princ Prog 1990, 25, 17–43.
17. Gayathri, C.; Bothner-By, A. A.; van Zijl, P. C. M.; MacLean, C. Chem Phys Lett 1982, 87, 192–196.
18. van Zijl, P. C. M.; Ruessink, B. H.; Bulthuis, J.; MacLean, C. Acc Chem Res 1984, 17, 172–180.
19. Emsley, I. W.; Lindon, J. C. NMR Spectroscopy Using Liquid Crystal Solvents; Pergamon Press: Oxford, 1975.
20. Diehl, P.; Khetrapal, C. L. NMR: Basic Principles and Progress, Vol. 1; Springer-Verlag: New York, 1969.
21. Khetrapal, C. L.; Kunwar, A. C.; Tracey, A. G.; Diehl, P., Eds. NMR: Basic Principles and Progress. Springer-Verlag: Berlin, 1975.
22. Snyder, L. C. J Chem Phys 1965, 43, 4041–4050.
23. Saupe, A. Angew Chem Int Ed Engl 1968, 7, 97–112.
24. Lohman, J. A. B.; MacLean, C. Chem Phys 1978, 35, 269–274.
25. Bothner-By, A. A. In Encyclopedia of Nuclear Magnetic Resonance; Grant, D. M.; Harris, R. K., Eds.; Wiley: Chichester, 1995; pp 2932–2938.
26. MacDonald, D.; Lu, P. Curr Opin Struct Biol 2002, 12, 337–343.
27. Latham, M. P.; Brown, D. J.; McCallum, S. A.; Pardi, A. Chembiochem 2005, 6, 1492–1505.
28. Lipsitz, R. S.; Tjandra, N. Annu Rev Biophys Biomol Struct 2004, 33, 387–413.
29. Prestegard, J. H.; Bougault, C. M.; Kishore, A. I. Chem Rev 2004, 104, 3519–3540.
30. Bax, A.; Grishaev, A. Curr Opin Struct Biol 2005, 15, 563–570.
31. Blackledge, M. Prog Nucl Magn Reson Spectrosc 2005, 46, 23–61.
32. Tolman, J. R.; Ruan, K. Chem Rev 2006, 106, 1720–1736.
33. Tolman, J. R.; Al-Hashimi, H. M.; Kay, L. E.; Prestegard, J. H. J Am Chem Soc 2001, 123, 1416–1424.
34. Losonczi, J. A.; Andrec, M.; Fischer, M. W. F.; Prestegard, J. H. J Magn Reson 1999, 138, 334–342.
35. Tjandra, N. Struct Fold Des 1999, 7, R205–R211.
36. Prestegard, J. H.; Kishore, A. I. Curr Opin Chem Biol 2001, 5, 584–590.
37. Tolman, J. R.; Al-Hashimi, H. M. In Annual Reports on NMR Spectroscopy; Webb, G. A., Ed.; Academic Press: New York, 2003; pp 105–166.
38. Tjandra, N.; Bax, A. Science 1997, 278, 1111–1114.
39. Ram, P.; Prestegard, J. H. Biochim Biophys Acta 1988, 940, 289–294.
40. Sanders, C. R.; Hare, B. J.; Howard, K. P.; Prestegard, J. H. Prog Nucl Magn Reson Spectrosc 1994, 26, 421–444.
41. Ottiger, M.; Bax, A. J Am Chem Soc 1998, 120, 12334–12341.
42. Hansen, M. R.; Mueller, L.; Pardi, A. Nat Struct Biol 1998, 5, 1065–1074.
43. Clore, G. M.; Starich, M. R.; Gronenborn, A. M. J Am Chem Soc 1998, 120, 10571–10572.
44. Hansen, M. R.; Hanson, P.; Pardi, A. Methods Enzymol 2000, 317, 220–240.

45. Sass, J.; Cordier, F.; Hoffmann, A.; Cousin, A.; Omichinski, J. G.; Lowen, H.; Grzesiek, S. J Am Chem Soc 1999, 121, 2047–2055.
46. Koenig, B. W.; Hu, J. S.; Ottiger, M.; Bose, S.; Hendler, R. W.; Bax, A. J Am Chem Soc 1999, 121, 1385–1386.
47. Sass, H. J.; Musco, G.; Stahl, S. J.; Wingfield, P. T.; Grzesiek, S. J Biomol NMR 2000, 18, 303–309.
48. Tycko, R.; Blanco, F. J.; Ishii, Y. J Am Chem Soc 2000, 122, 9340–9341.
49. Ruckert, M.; Otting, G. J Am Chem Soc 2000, 122, 7793–7797.
50. Alvarez-Salgado, F.; Desvaux, H.; Boulard, Y. Magn Reson Chem 2006, 44, 1081–1089.
51. Zweckstetter, M.; Bax, A. J Biomol NMR 2001, 20, 365–377.
52. Wu, B.; Petersen, M.; Girard, F.; Tessari, M.; Wijmenga, S. S. J Biomol NMR 2006, 35, 103–115.
53. Zweckstetter, M.; Hummer, G.; Bax, A. Biophys J 2004, 86, 3444–3460.
54. Ishii, Y.; Markus, M. A.; Tycko, R. J Biomol NMR 2001, 21, 141–151.
55. Ramirez, B. E.; Bax, A. J Am Chem Soc 1998, 120, 9106–9107.
56. Al-Hashimi, H. M.; Valafar, H.; Terrell, M.; Zartler, E. R.; Eidsness, M. K.; Prestegard, J. H. J Magn Reson 2000, 143, 402–406.
57. Tolman, J. R. J Am Chem Soc 2002, 124, 12020–12030.
58. Peti, W.; Meiler, J.; Bruschweiler, R.; Griesinger, C. J Am Chem Soc 2002, 124, 5822–5833.
59. Bondensgaard, K.; Mollova, E. T.; Pardi, A. Biochemistry 2002, 41, 11532–11542.
60. Zhang, Q.; Sun, X.; Watt, E. D.; Al-Hashimi, H. M. Science 2006, 311, 653–656.
61. Bastiaan, E. W.; Maclean, C.; Van Zilij, P. C. M.; Bothner-By, A. A. Ann Rep NMR Spec 1987, 19, 35–77.
62. Kung, H. C.; Wang, K. Y.; Goljer, I.; Bolton, P. H. J Magn Reson B 1995, 109, 323–325.
63. Tolman, J. R.; Flanagan, J. M.; Kennedy, M. A.; Prestegard, J. H. Proc Natl Acad Sci USA 1995, 92, 9279–9283.
64. Tjandra, N.; Omichinski, J. G.; Gronenborn, A. M.; Clore, G. M.; Bax, A. Nat Struct Biol 1997, 4, 732–738.
65. Prestegard, J. H.; Tolman, J. R.; Al-Hashimi, H. M.; Andrec, M. In Biological Magnetic Resonance; Krishna, N. R.; Berliner, L. J., Eds.; Plenum: New York, 1999; pp 311–355.
66. van Buuren, B. N.; Schleucher, J.; Wittmann, V.; Griesinger, C.; Schwalbe, H.; Wijmenga, S. S. Angew Chem Int Ed Engl 2004, 43, 187–192.
67. Tolman, J. R.; Prestegard, J. H. J Magn Reson B 1996, 112, 245–252.
68. Tjandra, N.; Grzesiek, S.; Bax, A. J Am Chem Soc 1996, 118, 6264–6272.
69. Al-Hashimi, H. M.; Majumdar, A.; Gorin, A.; Kettani, A.; Skripkin, E.; Patel, D. J. J Am Chem Soc 2001, 123, 633–640.
70. Zhang, Q.; Throolin, R.; Pitt, S. W.; Serganov, A.; Al-Hashimi, H. M. J Am Chem Soc 2003, 125, 10530–10531.
71. Al-Hashimi, H. M.; Tolman, J. R.; Majumdar, A.; Gorin, A.; Patel, D. J. J Am Chem Soc 2001, 123, 5806–5807.
72. Al-Hashimi, H. M.; Gorin, A.; Majumdar, A.; Patel, D. J. J Am Chem Soc 2001, 123, 3179–3180.
73. Bryce, D. L.; Boisbouvier, J.; Bax, A. J Am Chem Soc 2004, 126, 10820–10821.
74. D'Souza, V.; Dey, A.; Habib, D.; Summers, M. F. J Mol Biol 2004, 337, 427–442.
75. Kim, I.; Lukavsky, P. J.; Puglisi, J. D. J Am Chem Soc 2002, 124, 9338–9339.
76. Meiler, J.; Prompers, J. J.; Peti, W.; Griesinger, C.; Bruschweiler, R. J Am Chem Soc 2001, 123, 6098–6107.
77. Briggman, K. B.; Tolman, J. R. J Am Chem Soc 2003, 125, 10164–10165.
78. Clore, G. M.; Gronenborn, A. M.; Tjandra, N. J Magn Reson 1998, 131, 159–162.
79. Clore, G. M.; Gronenborn, A. M.; Bar, A. J Magn Reson 1998, 133, 216–221.
80. Clore, G. M.; Schwieters, C. D. Biochemistry 2004, 43, 10678–10691.
81. Schwieters, C. D.; Clore, G. M. Biochemistry 2007, 46, 1152–1166.
82. Trantirek, L.; Urbasek, M.; Stefl, R.; Feigon, J.; Sklenar, V. J Am Chem Soc 2000, 122, 10454–10455.
83. Mollova, E. T.; Hansen, M. R.; Pardi, A. J Am Chem Soc 2000, 122, 11561–11562.
84. Sibille, N.; Pardi, A.; Simorre, J. P.; Blackledge, M. J Am Chem Soc 2001, 123, 12135–12146.
85. Al-Hashimi, H. M.; Gosser, Y.; Gorin, A.; Hu, W.; Majumdar, A.; Patel, D. J. J Mol Biol 2002, 315, 95–102.
86. Al-Hashimi, H. M.; Gorin, A.; Majumdar, A.; Gosser, Y.; Patel, D. J. J Mol Biol 2002, 318, 637–649.
87. McCallum, S. A.; Pardi, A. J Mol Biol 2003, 326, 1037–1050.
88. Musselman, C.; Pitt, S. W.; Gulati, K.; Foster, L. L.; Andricioaei, I.; Al-Hashimi, H. M. J Biomol NMR 2006, 36, 235–249.
89. Klein, D. J.; Schmeing, T. M.; Moore, P. B.; Steitz, T. A. EMBO J 2001, 20, 4214–4221.
90. Olson, W. K.; Bansal, M.; Burley, S. K.; Dickerson, R. E.; Gerstein, M.; Harvey, S. C.; Heinemann, U.; Lu, X.,Neidle, S.; Sakked, Z.; Sklenar, H.; Suzuki, M.; Tung, C.; Weshof, E.; Wolberger, C.; Berman, H. M. J Mol Biol 2001, 313, 229–237.
91. Neidle, S. Oxford Handbook of Nucleic Acid Structure; Oxford University Press: New York, 1999.
92. Dingley, A. J.; Grzesiek, S. J Am Chem Soc 1998, 120, 8293–8297.
93. Pervushin, K.; Ono, A.; Fernandez, C.; Szyperski, T.; Kainosho, M.; Wuthrich, K. Proc Natl Acad Sci USA 1998, 95, 14147–14151.
94. Al-Hashimi, H. M.; Pitt, S. W.; Majumdar, A.; Xu, W.; Patel, D. J. J Mol Biol 2003, 329, 867–873.
95. Pitt, S. W.; Majumdar, A.; Serganov, A.; Patel, D. J.; Al-Hashimi, H. M. J Mol Biol 2004, 338, 7–16.
96. Pitt, S. W.; Zhang, Q.; Patel, D. J.; Al-Hashimi, H. M. Angew Chem Int Ed Engl 2005, 44, 3412–3415.
97. Reiter, N. J.; Blad, H.; Abildgaard, F.; Butcher, S. E. Biochemistry 2004, 43, 13739–13747.
98. Showalter, S. A.; Baker, N. A.; Tang, C. G.; Hall, K. J Biomol NMR 2005, 32, 179–193.
99. Musselman, C.; Al-Hashimi, H. M.; Andricioaei, I. Biophys J 2007, in press.
100. Tolman, J. R.; Flanagan, J. M.; Kennedy, M. A.; Prestegard, J. H. Nat Struct Biol 1997, 4, 292–297.
101. Pervushin, K.; Riek, R.; Wider, G.; Wuthrich, K. J Am Chem Soc 1998, 120, 6394–6400.
102. Ying, J.; Grishaev, A.; Bryce, D. L.; Bax, A. J Am Chem Soc 2006, 128, 11443–11454.
103. Hansen, A. L.; Al-Hashimi, H. M. J Magn Reson 2006, 179, 299–307.

104. Grishaev, A.; Ying, J.; Bax, A. J Am Chem Soc 2006, 128, 11443–1154.
105. Boisbouvier, J.; Bryce, D. L.; O'Neil-Cabello, E.; Nikonowicz, E. P.; Bax, A. J Biomol NMR 2004, 30, 287–301.
106. Miclet, E.; O'Neil-Cabello, E.; Nikonowicz, E. P.; Live, D.; Bax, A. J Am Chem Soc 2003, 125, 15740–15741.
107. Miclet, E.; Boisbouvier, J.; Bax, A. J Biomol NMR 2005, 31, 201–216.
108. O'Neil-Cabello, E.; Bryce, D. L.; Nikonowicz, E. P.; Bax, A. J Am Chem Soc 2004, 126, 66–67.
109. Schwalbe, H.; Marino, J. P.; King, G. C.; Wechselberger, R.; Bermel, W.; Griesinger, C. J Biomol NMR 1994, 4, 631–644.
110. Ottiger, M.; Delaglio, F.; Bax, A. J Magn Reson 1998, 131, 373–378.
111. Vallurupalli, P.; Moor, P. B. J Biomol NMR 2002, 24, 63–66.
112. Yan, J.; Corpora, T.; Pradhan, P.; Clore, J. H. J Biomol NMR 2002, 22, 9–20.
113. Zidek, L.; Wu, H.; Feigon, J.; Sklenar, V. J Biomol NMR 2001, 21, 153–160.
114. Brutscher, B.; Boisbouvier, J.; Pardi, A.; Marion, D.; Simorre, J. P. J Am Chem Soc 1998, 120, 11845–11851.
115. Jaroniec, C. P.; Boisbouvier, J.; Tworowska, I.; Nikonowicz, E. P.; Bax, A. J Biomol NMR 2005, 31, 231–241.
116. Varani, G.; Aboulela, F.; Allain, F. H. T. Prog Nucl Magn Reson Spectrosc 1996, 29, 51–127.
117. Wijmenga, S. S.; van Buuren, B. N. M. Prog Nucl Magn Reson Spectrosc 1998, 32, 287–387.
118. Furtig, B.; Richter, C.; Wohnert, J.; Schwalbe, H. Chembiochem 2003, 4, 936–962.
119. Lukavsky, P. J.; Kim, I.; Otto, G. A.; Puglisi, J. D. Nat Struct Biol 2003, 10, 1033–1038.
120. Du, Z.; Yu, J.; Ulyanov, N. B.; Andino, R.; James, T. L. Biochemistry 2004, 43, 11959–11972.
121. Flodell, S.; Petersen, M.; Girard, F.; Zdunek, J.; Kidd-Ljunggren, K.; Schleucher, J.; Wijmenga, S. Nucleic Acids Res 2006, 34, 4449–4457.
122. Chen, Y.; Fender, J.; Legassie, J. D.; Jarstfer, M. B.; Bryan, T. M.; Varani, G. EMBO J 2006, 25, 3156–3166.
123. Richards, R. J.; Wu, H.; Trantirek, L.; O'Connor, C. M.; Collins, K.; Feigon, J. RNA 2006, 12, 1475–1485.
124. Leeper, T. C.; Varani, G. RNA 2005, 11, 394–403.
125. Staple, D. W.; Butcher, S. E. J Mol Biol 2005, 349, 1011–1023.
126. Getz, M. M.; Andrews, A. J.; Fierke, C. A.; Al-Hashimi, H. M. RNA 2006, 13, 251–266.
127. Sun, X.; Zhang, Q.; Al-Hashimi, H. M. Nucleic Acids Res 2007, 35, 1698–1713.
128. Puglisi, J. D.; Tan, R.; Calnan, B. J.; Frankel, A. D.; Williamson, J. R. Science 1992, 257, 76–80.
129. Aboul-Ela, F.; Karn, J.; Varani, G. Nucleic Acids Res 1996, 24, 3974–3981.
130. Zacharias, M.; Hagerman, P. J. Proc Natl Acad Sci USA 1995, 92, 6052–6056.
131. Long, K. S.; Crothers, D. M. Biochemistry 1999, 38, 10059–10069.
132. Ippolito, J. A.; Steitz, T. A. Proc Natl Acad Sci USA 1998, 95, 9819–9824.
133. Casiano-Negroni, A.; Sun, X.; Al-Hashimi, H. M. Biochemistry, 2007, 46, 6525–6535.
134. Zacharias, M.; Hagerman, P. J. J Mol Biol 1995, 247, 486–500.
135. Zacharias, M.; Hagerman, P. J. J Mol Biol 1996, 257, 276–289.
136. Kim, H. D.; Nienhaus, G. U.; Ha, T.; Orr, J. W.; Williamson, J. R.; Chu, S. Proc Natl Acad Sci USA 2002, 99, 4284–4289.
137. Rueda, D.; Wick, K.; McDowell, S. E.; Walter, N. G.; Jeong, S.; Sefcikova, J.; Tinsley, R. A.; Engelke, D. R.; Harris, D. A.; Pereira, M. J. Biochemistry 2003, 42, 9924–9936.
138. Woodson, S. A. Curr Opin Chem Biol 2005, 9, 104–109.
139. Lynch, S. R.; Puglisi, J. D. J Am Chem Soc 2000, 122, 7853–7854.
140. Du, Z.; Lind, K. E.; James, T. L. Chem Biol 2002, 9, 707–712.
141. Faber, C.; Sticht, H.; Schweimer, K.; Rosch, P. J Biol Chem 2000, 275, 20660–20666.
142. Aboul-Ela, F.; Karn, J.; Varani, G. J Mol Biol 1995, 253, 313–332.
143. Murchie, A. I.; Davis, B.; Isel, C.; Afshar, M.; Drysdale, M. J.; Bower, J.; Potter, A. J.; Starkey, I. D.; Swarbrick, T. M.; Mirza, S.; Prescott, C. D.; Vaglio, P.; Aboul-Ela, F.; Karn, J. J Mol Biol 2004, 336, 625–638.
144. Reiter, N. J.; Nikstad, L. J.; Allmann, A. M.; Johnson, R. J.; Butcher, S. E. RNA 2003, 9, 533–542.
145. Vermeulen, A.; McCallum, S. A.; Pardi, A. Biochemistry 2005, 44, 6024–6033.
146. Du, Z.; Ulyanov, N. B.; Yu, J.; Andino, R.; James, T. L. Biochemistry 2004, 43, 5757–5771.

Reviewing Editor: Nils Walter